Journal of Thermal Analysis and Calorimetry, Vol. 91 (2008) 2, 427–436

SURFACE LASER SINTERING OF EXOTHERMIC POWDER COMPOSITIONS
A thermal and SEM/EDX study

I. V. Shishkovsky[1*], *V. I. Scherbakov*[1], *Y. G. Morozov*[2], *M. V. Kuznetsov*[2] *and I. P. Parkin*[3]

[1]P.N. Lebedev Physical Institute (LPI), Samara Branch, Russian Academy of Sciences, Samara, 443011 Russia
[2]Institute of Structural Macrokinetics and Materials Science Russian Academy of Sciences (ISMAN), Chernogolovka Moscow region, 142432 Russia
[3]Department of Chemistry, University College London (UCL), 20 Gordon Street, London WC1H 0AJ UK

This work reports the temperature behavior associated with formation of new metal-polymer, intermetallic, and ceramic materials by Selective Laser Sintering. Here, experimental data produced from temperature measurements for inert as well as reaction powder compositions and the combustion wave front is reported. Analysis using an analog-digital-analog computer converter allowed some control of laser movement and hence some control of the exothermal reaction – in so doing it provided near optimum conditions for forming layered 3D articles.

Keywords: *EDX, exothermic powder compositions, microstructure, selective laser sintering, self-propagating high-temperature synthesis, SEM, thermocouple measurements*

Introduction

Self-propagating high-temperature synthesis (SHS) is an exothermic solid-state reaction of powder composites. It provides a rapid, low external energy route for the formation of uncommon (metastable) phases and functionally graded compositions. A factor limiting the wide spread use of SHS for various applications is a lack of control. Further limitations of SHS in the formation of 'net-shape' products are (*i*) its multistage character and (*ii*) its high sometimes uncontrollable exothermicity – it is normally a controlled or sometimes uncontrolled explosion.

One of the ways for controlling SHS is the application of an external physical field especially of electromagnetic origin. After appropriate choice of the frequency/amplitude of an applied field the combustion parameters such as velocity and temperature within an SHS process can be influenced. Previously we have shown that an external electromagnetic field not only contributes an additional heat source due to Joule heating but also affects the interaction mechanisms, the structure and the chemical composition of the final product [1]. The non-thermal heating affect of an external electromagnetic field during SHS is related to the specific system under study due to differences in movement of defects and ions at the 'plasma-like' molten wave front.

Selective laser sintering (SLS) is one of the most commercially developed methods within rapid prototyping and manufacturing (RP&M) technology. This method allows production of three-dimensional parts by using a spatially selective laser irradiation (LI) (compare with no local controlling microwave sintering [2]) on the surface of powder compositions [3–5]. The direct formation of functional materials and tools of the required shape is a distinctive feature of SLS. New directions in SLS method development can be found by overlapping the SLS process with SHS [5]. This was first accomplished at the Samara branch of LPI. In this case, under optimum conditions the SHS reaction is only initiated within the spot of the focused laser beam. The SHS reaction can then 'anticipate' or 'lag behind' the sintering process itself. In this case the green mixture component may be fused or incompletely reacted. Thus, the main task of any synthesis employing laser energy is selection of the laser sintering conditions at which both of the processes – SHS and SLS will be in dynamic equilibrium.

Three-dimensional (3D) products synthesized using an SHS reaction have complex physical-mechanical properties that cannot be obtained by using conventional synthetic methods. To date, SLS has been used for the following SHS systems:

- mixture of metals for intermetallide synthesis: Ni+Ti [6], Ni+Al [7], Ti+Al [8] ;

* Author for correspondence: shiv@fian.smr.ru

1388–6150/$20.00

Akadémiai Kiadó, Budapest, Hungary
Springer, Dordrecht, The Netherlands

- mixture of oxides for ceramics synthesis: TiO_2+ZrO_2+PbO [9], Al(Al_2O_3)+Zr(ZrO_2) [10];
- mixture of oxides and metals for ferrites synthesis: BaO_2+Fe_2O_3+Cr_2O_3+Fe, Li_2CO_3+ Fe_2O_3+Cr_2O_3+Fe, and $SrFe_{12}O_{19}$ [11];
- high-temperature superconducting (HTSC) oxide ceramics $YBa_2Cu_3O_7$ [3].

Previously we have developed and refined the testing scheme for electro-thermal phenomena studies which can directly influence the SHS combustion wave front. Data treatment using a computerized analog-digital converter was achieved [12]. In this paper the data produced by temperature measurements during SLS for inert compounds, as well as for the reaction-capable powder compositions are described. Comparative results of structural-phase transformation during laser controlled SHS in reaction-capable compositions are also presented.

Experimental setup and measurement technique

All the powder reagents were obtained from the Russian Chemical Market and used as supplied. All the powder fractions had particles sizes that were less than 60 μm. Our experimental setup for the SLS of powder composites involves: (1) continuous wave YAG : Nd^{3+} laser; (b) deflectors for the laser beam to scan the X–Y plane; (c) personal computer (PC); (d) interchangeable lenses with f~149 and 336 mm (in order to obtain focused spots with D~50 and 100 mm, respectively); (e) mechanism for deposition and leveling of the powder mixture and (f) vertically traveling cylindrical platform. The laser beam can scan an area of 50·50 or 100·100 mm and was controlled by PC through mechanical deflectors. The laser beam power P could be varied from 0.5 to 25 W. Laser sintering was induced in air, argon or nitrogen depending on each particular powder mixture. Laser scanning of the surface powder was realized via meander mode.

Diagrams of the setup for electrical and thermal measurements during laser controlled SHS-processes are shown in Fig. 1. Powder compositions were placed on a metal platform. The volume of cuvette was ~12 cm^3. The dimensions of the LI zone were 10·30 mm with a typical sintered monolayer depth of 0.5–3 mm. Thermocouples were inserted into the powder within this zone 5 mm from the zone edge at a depth of 3–5 mm. Reference and recording elements were arranged in the unified measuring cell. It ensures the elimination of boundary influences on the combustion front propagation and allowed the simultaneous determination of the thermal and kinetic characteristics of the process. The thermocouple junctions

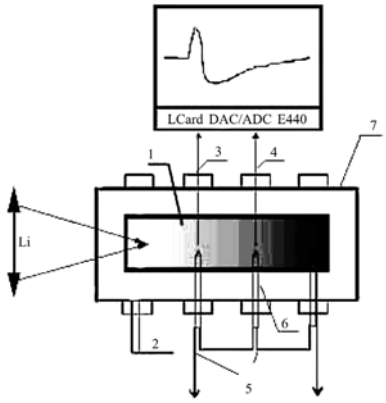

Fig. 1 Setup of thermo-electrical measurements in SHS powdered mixes. 1 – studied blend, 2 – inputs for measuring devices, 3 – reference probe, 4 – registered probe, 5 – thermocouples, 6 – insulators, 7 – cuvette

were located near to each electrode. For the intermetallic synthesis chromel-copel thermocouples (temperature range 200–1100°C) were used, and for the other reactions thermocouples with higher temperature ranges – W+Re (5%)–W+Re (20%) thermocouple (range 400–2800°C) were used. The laser was applied from the top of the platform. The experimental error in the measurements (°C) was: chromel-copel ±3–5°C; a tungsten-rhenium ±0.1–4°C. A 16 channel DAC/ADC E-440 external module (connected with PC via USB2.0) was used for digitization of experimental data in accordance to the scheme shown in Fig. 1. Its technical characteristics are reported on the website of the Joint-Stock Company 'L-Card' (<http:// www.lcard.ru/e-440.php3>).

Measurements of the temperature distribution were conducted near the laser-sintering zone (one monolayer in volume of the powder mixture). These measurements depended upon the laser configurations such as power, scanning velocity and spot diameter. Both SHS reaction capable systems – Ni–Ti, Ni–Al, Ti–Al, and combustion of titanium in air as well as SHS inert systems such as iron powder (PJ RNL-A grade), metal–polymer powder composition were studied. The Ni base cladding powder (grade PGSR4 with ~80% Ni, and cladding additives in balance – 1.5–3.8 B; 0.6–1.0 C; 2.0–4.5 Si; 12–18 Cr; ≤5.0 Fe; 0.04 P; 0.04 S, mass%) was used for intermetallic synthesis as in the mixture with a polyamide (grade P12) in a proportion 4:1. All the powders have a dispersion of less than 63 μm except for iron powder which was 100–200 μm.

In Figs 2 and 3 the reaction mixture before propagation is shown, enabling the position of the thermocouples within the system to be seen.

Data regarding the geometrical location of the thermocouples showing how a sintered monolayer (a_i, b_i) varied with LI conditions and powder composi-

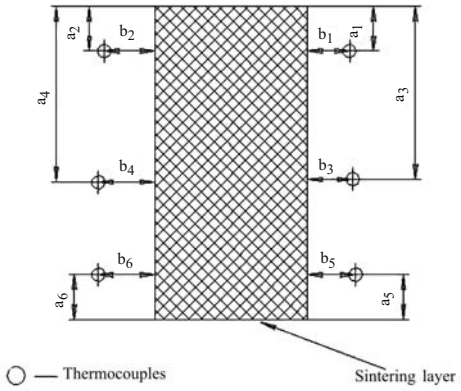

Fig. 2 Scheme of thermocouples distribution (i=1..6, a_i, b_i – sizes), relative the zone (hatching marked) of sintering

Fig. 3 Appearance (top) of cuvette for sintering of powders, pointers shows the thermocouple places

tions is listed in Table 1. In the last three columns the dimensions of the sintering zone and its depth for those sintered regimes are presented. No entry in the table means that layer sintering was not successful and we had an uncontrolled thermal explosion. Table 1 also contains experimental details of the LI set-up including power, scanning velocity, time of sintering as set by the PC program 'SINTER' diagnostic. In reality the process of temperature digitization required much longer (column 5, Table 1) than the sintering time. Comparison of data from the SINTER program (column 2) and the digitization L-Card (column 5) shows, that the process times are essentially different. It is related to the difference in PC clock rates (which uses data from the SINTER program for determining the LI movement) and signal processor rates from the DAC/ADC. Therefore it was necessary to apply a correcting multiplier, matching these parameters (in our case it was experimental determined ~1.14). The spot size for SLS for the metal-polymer mixtures was little bit more than that shown in Table 1. It is related to the drift from the laser focus at a distance of 20 mm. The optimum SLS regime for 3D sample synthesis from such powder compositions has been previously determined [13].

Temperature measurement results

In Figs 4–14 digitization results for the temperatures recorded by thermocouples for the laser treatment of different powder compositions are presented. The number of the curve corresponds to the specific thermocouple number (as shown in Fig. 3).

Figures 4–9 describe the temperature distribution in the inert powder compositions. In these cases, of course, sintering without reactions is realized only at the laser spot. SHS propagation beyond the laser point source is not observed.

Figures 10–17 described the character of temperature distribution in the reactive capable powder compositions – where SHS propagation waves can move in front of the laser beam.

Regimes of laser influence in Figs 10–13 and 15 correspond to the experimentally determined conditions for laser controlled overlap of the SLS and SHS processes. Figures 14, 16 and 17 describes these processes, which were carried out in the thermal explosion regime.

In those cases, when monolayer sintering was successful (Figs 4–13 and 15), the last column in Table 1 reports the thicknesses of the sintered layer. As thermocouples were situated on the periphery of sintering, absolute values of temperatures are not

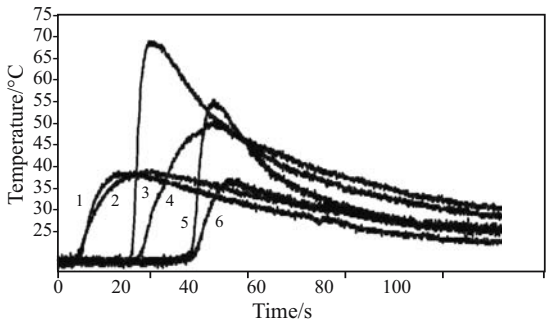

Fig. 4 Laser sintering of metal-polymer powder mixture PGSR4+polyamide in 4:1 ratio. Laser scan velocity V=15.6 cm s^{-1}, beam diameter d=50 μm, laser power P=6.6 W. (Here is and below all number of curves are according to number of thermocouples from Fig. 3)

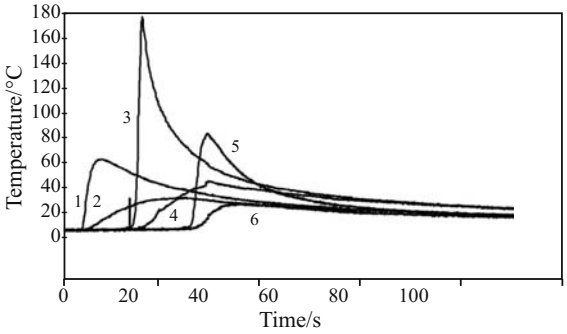

Fig. 5 The same as in Fig. 4 except P=10.7 W

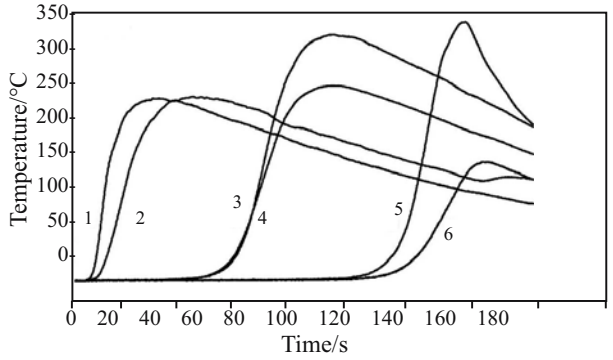

Fig. 6 Laser sintering of iron powder (PJ RNL-A grade). Laser scan velocity V=5.7 cm s^{-1}, beam diameter d=50 μm, laser power P=23.5 W

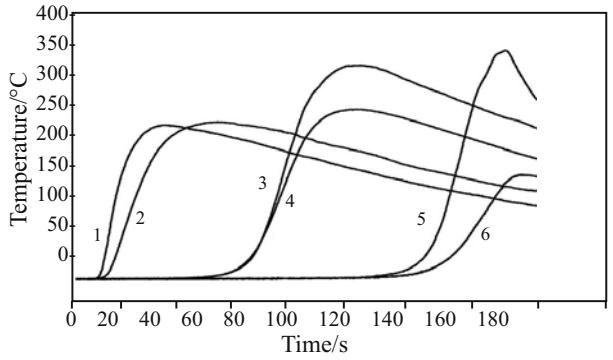

Fig. 7 The same as in Fig. 6 except P=29.5 W

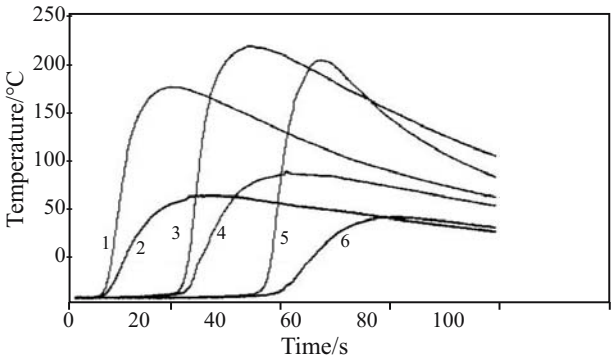

Fig. 8 Laser sintering of iron powder (PJ RNL-A grade). Laser scan velocity V=5.7 cm s^{-1}, beam diameter d=100 μm, laser power P=23.9 W

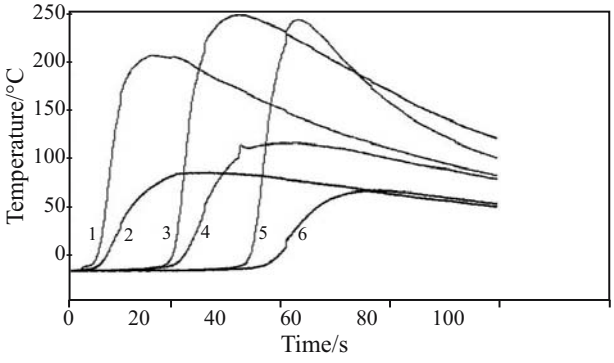

Fig. 9 The same as in Fig. 7 except P=30.3 W

high. The SEM and X-ray phase analysis after reaction shows that chemical transformation occurs in the case of reactive powders. Moreover, those phases intended to be made beforehand at the experimental design stage were actually made.

In the case of a thermal explosion, all the powder volume (~12 cm^3) was burned through completely, however the contact points to the thermoelectric junction were not destroyed. This allowed us to register the temperature changing with time for the whole process.

As a whole, the temperature profiles had an understandable sequence for all of the experiments (Figs 4–17). The first response was always from the first thermocouple, which was positioned closest to the starting point for initiation of laser scanning. The second (counter) thermocouple routinely behind the reaction front does not record a temperature increase until some time later. Measurements from the 3rd and 4th thermocouples are comparable with first one. It is connected as follows: when the reaction front reaches the midpoint of the sintered monolayer (Fig. 3), the powder volume is already very hot. If reaction control is lost, the temperature measurements for the 3rd and 4th thermocouples are maximized. Finally reaction exothermicity is registered from the 5th and 6th thermocouples which are further away from the initiation point.

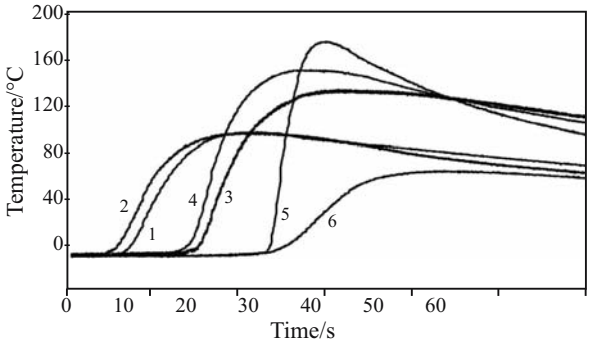

Fig. 10 Laser sintering of powder composition Ni (PGSR)+Al (ASD4)=3:1 ratio. Laser scan velocity V=11.4 cm s^{-1}, beam diameter d=100 μm, laser power P=23.9 W

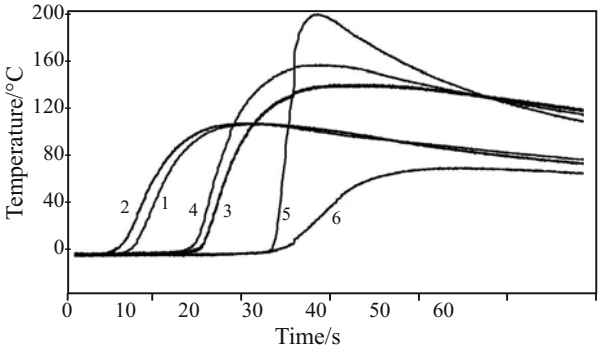

Fig. 11 The same as in Fig. 10 except P=30.3 W

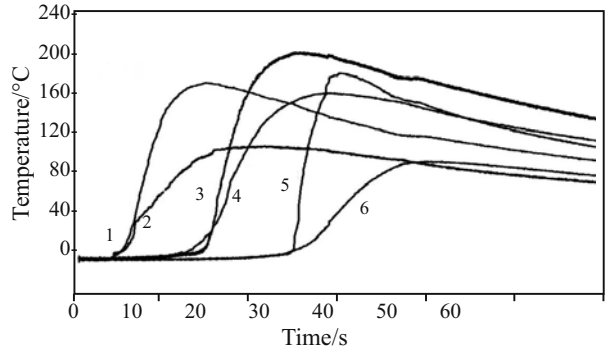

Fig. 12 Laser sintering of powder composition Ni (PGSR4)+Ti (PTOM)=1:1 ratio. Laser scan velocity V=11.4 cm s^{-1}, beam diameter d=100 μm, laser power P=23.9 W

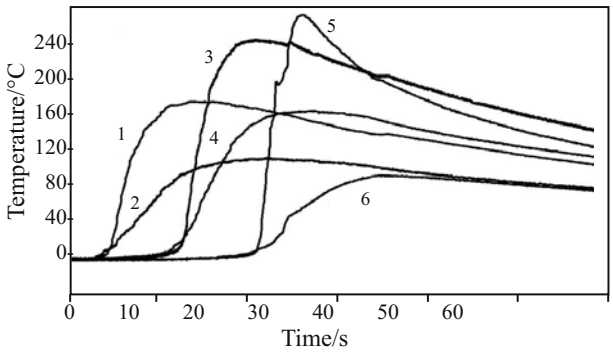

Fig. 13 The same as in Fig. 12 except P= 30.3 W

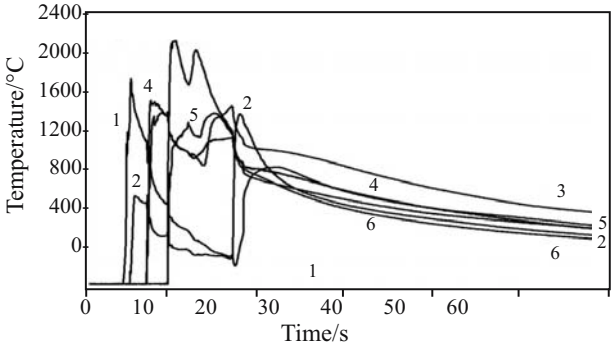

Fig. 14 Laser sintering of powder composition Ni+Al (ASD4)=1:1, beam diameter d=100 μm. Laser regime P=8 W, V=11.4 cm s^{-1} – pure nickel (PNK grade)

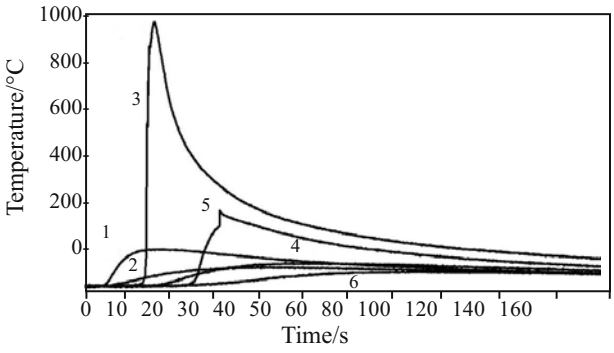

Fig. 15 The same as in Fig. 14 except: laser regime V=2.9 cm s^{-1}, P=30.2 W – Ni cladding powder (PGSR4 grade)

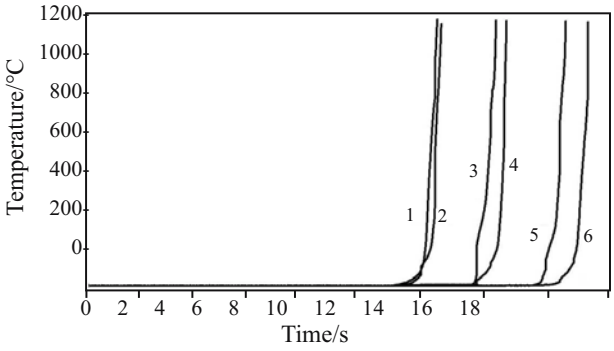

Fig. 16 Laser power P=30.3 W. Chromel-copel thermocouples. Laser sintering of pure titanium in air. Scan velocity V=5.7 cm s^{-1}, beam diameter d=100 μm

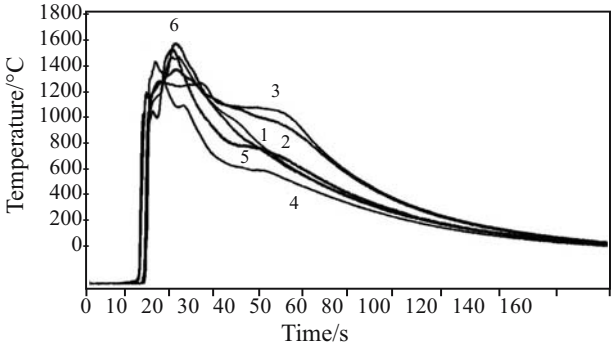

Fig. 17 Sintering titanium on air. Laser beam is defocus (d~5 mm) and stay in center. Laser power P=5.8 W

In Figs 18–20 the results of monolayer sintering are presented; Fig. 18 corresponds to the completely sintered inert metal-polymer mixture in Fig. 19 it is visible, that in the laser scan region, the upper zero corner got heated during the quickest possible time; Fig. 20 represents a bulk sample, obtained for a reaction of the uncontrolled, explosive type. A two dimensional transient theoretical model of laser sintering of the reactive powder compositions with allowance for chemical reaction kinetics has been reported previously [14] by us. The experimental data obtained in this study provides a good basis for comparing the numerical and experimental approach.

Microstructural and phase analysis of sintering results

It is known, that in conventional SHS the process can proceed by several mechanisms level-by-level (frontal) combustion, spin combustion, volume thermal explosion. Thus if the strong self-heating of a system is supervised, temperatures close to the calculated adiabatic temperature of the complete exothermic chemical transformation, are obtained. For the technology

Table 1 Experimental results of monolayer sintering and thermocouple position with respect to the sintered region

Comp. (focus size)	Sintering time (sinter)/s	Velocity V/cm s^{-1}	P/W	N item/ the end of treatment by (L'Card)/s	N°1		N°2		N°3		N°4		N°5		N°6		Length/ mm	Width/ mm	Depth/ mm
					a1	b1	a2	b2	a3	b3	a4	b4	a5	b5	a6	b6			
					thermocouple situation														
Fe (149)	165.27	5.7	23.5	1,2, 3– 149/146.5/136	2.4	2.4	0.8	1.9	13.9	2	12.8	2.4	2.6	1.6	2.1	3	27.5	8.6	1.2
			29.9	1,2, 3– 147.5/147.5/148.5	2.5	2.3	0.9	1.8	14	1.9	12.9	2.3	2.6	1.5	2.1	2.9	27.6	8.8	1.4
Fe (336)	54.07	5.7	23.9	1– 46	2	1.3	0.8	3.3	13.2	1	12.8	3.6	5.3	0.6	4.8	4.6	30.2	8.5	1.2
				2, 3 –45/44.5	2	1	1.1	3.6	13.2	1	13.1	3.6	5.3	0.9	4.5	4.3			
			30.3	1, 2, 3–45/43.5/41.5	2.1	1.1	1.1	3.4	13.3	1	13.1	3.5	5.3	0.8	4.6	4.2	30.3	8.6	1.3
NiTi (336)	29.95	11.4	23.9	1, 2, 3–29/25.5/29	2.2	1.9	1.1	2.7	13.4	1.3	12.8	2.4	3.4	1.1	3	3.6	28.8	8.8	1.6
			30.3	1, 2, 3–29/26/25.5	2.3	1.8	1.2	2.6	13.5	1.2	12.9	2.3	3.5	1	3.1	3.5	29	9	1.7
PN + PA (149+20 mm)	34.24	15.6	6.6	1, 2– 30/31.5	2.5	1.5	2.8	2.1	15.2	0.5	13.8	1.5	0.6	0.4	0.8	2.5	26.3	10.1	1.2
				3– 31.5	1.5	2.5	1.8	1.1	14.2	1.5	12.8	0.5	0.4	1.4	1.8	1.5			
			10.7	1–29	1.3	2.3	1.6	0.8	14	1.3	12.6	0.2	1.3	1.2	2.7	1.2	27	10.6	1.6
				2–29.5	1.9	2.5	2.2	0.6	14.6	1.5	13.2	0	0.7	1.4	2.1	1			
				3– 29	0.9	2.2	1.2	0.9	13.6	1.2	12.2	0.3	1.7	1.1	3.1	1.3			
Ni_3Al (336)	29.95	11.4	23.9	1, 2, 3–28.5/28/26	2.6	1.9	1.6	1.6	13.8	1.7	13.6	1.4	4.2	1.4	3.9	2.4	29.8	9.5	1.8
			30.3	1, 2,3–25.5/29/26	2.7	1.9	1.7	1.6	13.9	1.6	13.7	1.4	4.3	1.3	4	2.4	30	9.6	2
NiAl (336)	21.98	2.9	30.2	1–	2.5	0.5	2.7	2	–	–	–	–	6	0.6	5.8	4.4	33	7.7	–

Notes:
– For powder compositions in Table 1 SLS was realized in the argon environment, excepting of iron and metal-polymer powder system PN+PA
– Sintering time (sinter) / column – 2/ is real time, during which the laser beam scanned by surface of the powder
– L'Card time / column – 5, after bar/ is a time, during which the DAC/ACD module was turned on

of layer by layer SLS of 3D parts from reactive powder compositions, those conditions are completely unacceptable (see temperature behavior in Figs 14–17), as they are all unchecked combustions of the volume of a powder. It carries on to the complete loss of the shape of a synthesized part (compare Figs 9 and 20). By lowering the exothermicity of an SHS reaction it should be possible to enable the SLS to only ignite the reaction at the laser spot [7, 8]. Therefore it is important to be convinced as to the formation of the new chemical compounds at the measured temperatures and to estimate the depth of chemical transformation during SLS+SHS.

Microstructure and element analysis of phase composition of sintered samples was examined after the combined SLS+SHS process by means of scanning electronic microscope – LEO 1450 (accelerating voltage 20 kV), equipped with Energy Dispersive X-ray Microanalysis (INCA ENERGY 300, Oxford Instruments). The synthesized monolayer samples were prepared from Ni–Ti=1:1, Ni–Al=3:1 compositions and confirmed as the correct composition in the products by microanalysis. Intermetallic SHS reactions often have a complex composition, so to the material synthesized during laser controlled SHS from Ni–Ti and Ni–Al mixtures. X-ray phase analysis showed the presence of NiTi and $NiTi_2$ in the Ni–Ti mixture [6]. In the Ni–Al case both Ni_3Al and NiAl were observed [7].

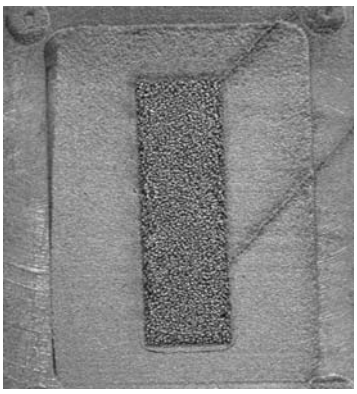

Fig. 18 Photograph of the product formed from the laser sintering of metal-polymer mixture. Places of input and output of laser beam are clearly shown. Regime treatment corresponds to Fig. 5. Monolayer in the volume of cuvette. Top view, laser scan has been made by rectangular meander

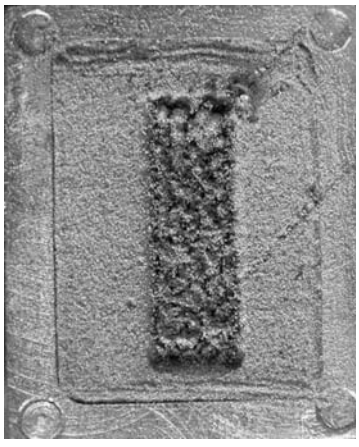

Fig. 19 Sintered monolayer of powder mixture Ni–Ti=1:1. Regime treatment corresponds to Fig. 6. Comments the same as for Fig. 18

The microstructure of the Ni-Ti mixture after SLS+SHS (Fig. 21) consists of large (~100 μm) particles of the newly formed intermetallic phases (Spectrum-S2) and small (~50 μm) particles of the initial powder (Spectrum-S1). The presence of the intermetallic compound testifies to the passage of the SHS reaction.

As seen from data in Table 2 (Spectrum-S2) the nickel to titanium ratios matches the stoichiometry of the intermetallic phase NiTi (nitinol). The presence of the other alloying elements is caused by the original composition of the starting PGSR4 powder. Element change by direction between two particles in Fig. 21 (line scan is shown superimposed in this Fig.) shows that the titanium and nickel traces mirror each other; this is expected for a structural – phase formation of new intermetallic phases from the reaction.

In Fig. 22 and Table 3 the results of SEM and EDX are represented in the same powder mixture (Ni+Ti=1:1), but at a higher laser power of LI P=30.3 W. As seen in Fig. 22 (line scan is also shown superimposed in this Fig.) the microstructure reaches even greater refinement in the SLS+SHS process when operated in this regime. So to eliminate a particle of the initial powders (Ni or Ti) from the formed intermetallic phases is very difficult.

The distribution of chemical elements is even more homogeneous and, evidently, the structure has a completely intermetallic nature. By correlation of Ti and Ni contents (see data in Table 3) in the structure

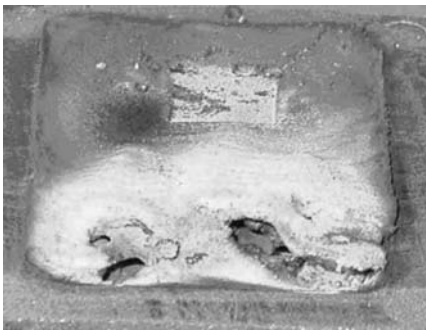

Fig. 20 Result of SLS with an uncontrollable SHS reaction. In the center it can be clearly seen the square area, in which sintering was proposed. Regime treatment corresponds to Fig. 13. Comments the same as for

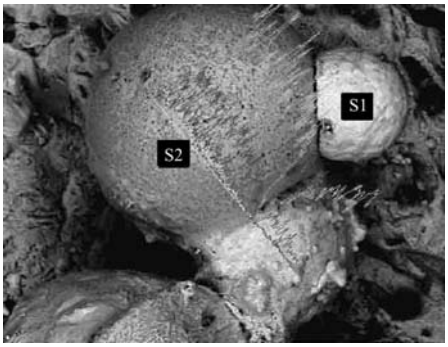

Fig. 21 Microstructure and element content after SLS+SHS in Ni–Ti mixture. Regime treatment corresponds to Fig. 12

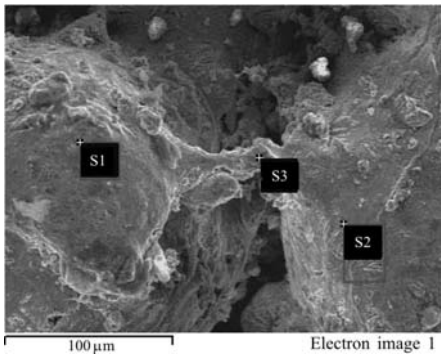

Fig. 23 Microstructure and element content after SLS in Ni–Al mixture. Regime of treatment corresponds to

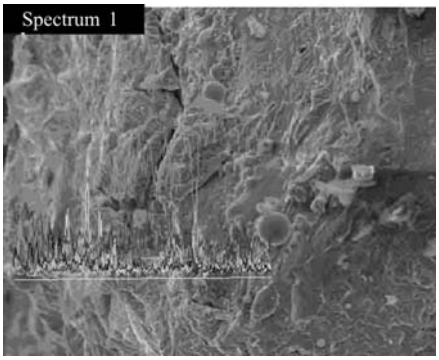

Fig. 22 Microstructure and element content after SLS in Ni–Ti mixture. Regime treatment corresponds to Fig. 13

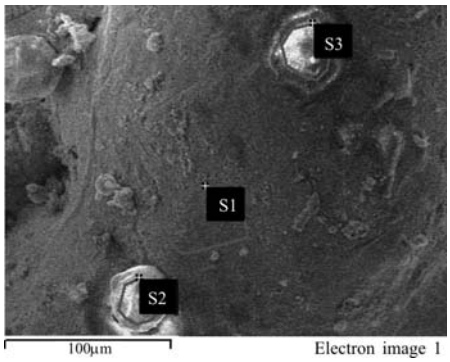

Fig. 24 Microstructure and element content after SLS in Ni–Al mixture. Regime of treatment corresponds to Fig. 11

of the intermetallic phases both NiTi, $NiTi_2$ are found. Thus, it is possible that the degree of chemical transformation reaches 100%. As the phase $NiTi_2$ phase is metastable, adding thermal annealing after SLS can reduce its content to zero [1, 6]. So, in the case of nitinol formation (phase NiTi) such as in a bioimplant material, the presence of the bioinert minor phase $NiTi_2$ is not critical.

In Figs 23, 24 and Tables 4, 5 the results of SEM and EDX for the laser control SHS of mixtures of Ni+Al=3:1 are presented. Here again, there is a formation of intermetallic phases NiAl and Ni_3Al. An increase of laser power up to 30.3 W, induces a microstructure (Fig. 24) which has a more homogeneous composition, though small 'droplets' (~30 µm) of low-melting aluminum remained on the surface of the intermetallic phases.

A microstructure study of intermetallic phases under higher magnification gives interesting results (Figs 25, 26). The surface of intermetallic compound

Table 2 EDX analyses of the particles shown in Fig. 21 – all elements are normalized in atomic percent

Spectrum	C	O	Al	Si	Ti	Cr	Fe	Ni	Total
S1	27.77	5.90		4.85	0.63	5.79	1.12	53.94	100.00
S2	32.97	16.58	2.71	1.45	23.68	4.32	0.75	17.54	100.00
Max.	32.97	16.58	2.71	4.85	23.68	5.79	1.12	53.94	
Min.	27.77	5.90	2.71	1.45	0.63	4.32	0.75	17.54	

Table 3 EDX analyses of the particles shown in Fig. 22 – all elements are normalized in atomic percent

Spectrum	C	O	Al	Si	Ca	Ti	Cr	Fe	Ni	Zr	Total
Spectrum 1	25.39	33.58	0.73	1.79	0.74	20.49	1.72	0.37	14.30	0.89	100.00
Max.	25.39	33.58	0.73	1.79	0.74	20.49	1.72	0.37	14.30	0.89	
Min.	25.39	33.58	0.73	1.79	0.74	20.49	1.72	0.37	14.30	0.89	

Table 4 EDX analysis of the particles shown in Fig. 23

Spectrum	C	O	Al	Cr	Ni	Total
S1	44.88	16.43	7.06	0.96	30.66	100.00
S2	32.22	29.11	12.56		26.11	100.00
S3	52.14	17.46	6.83		23.57	100.00
Max.	52.14	29.11	12.56	0.96	30.66	
Min.	32.22	16.43	6.83	0.96	23.57	

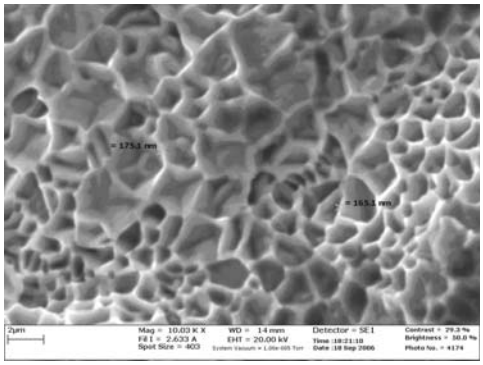

Fig. 25 Nanostructure after SLS in Ni–Ti mixture. Regime treatment corresponds to Fig. 13

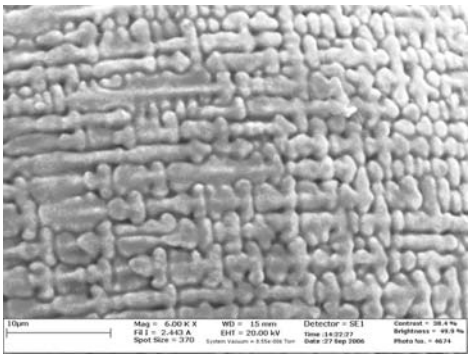

Fig. 26 Nanostructure after SLS in Ni–Al mixture. Regime treatment corresponds to Fig. 11

Table 5 EDX analysis of the particles shown in Fig. 24

Spectrum	O	Al	Ni	Total
S1	42.23	23.01	34.76	100.00
S2	36.16	15.52	48.32	100.00
S3	64.57	35.43		100.00
Max.	64.57	35.43	48.32	
Min.	36.16	15.52	34.76	

has strongly expressed fractal order [15]. Such order is observed in all samples synthesized at higher laser power.

The wall dimensions of the obtained fractal nano structures are ~165–175 nm in nitinol. It offers one more method of producing pores of nanometer width [16]. The cause of such behavior in intermetallic phases during the combined SLS+SHS process will be a subject of our future activity.

Thus, the study of microstructures and their element analysis shows that the SHS reaction is of the diffusive type. The essential advantage of the given SHS type is the possibility to produce net shape articles of pre-determined form. This includes the opportunity of making functionally-graded structures generated by computer design.

Conclusions

This present paper provides the first experimental results of the direct temperature measurement of selective laser sintering of SHS capable powders. It is possible to make conclusions about the behavior and mechanisms of the SHS process and to control the synthesis using an external laser source. The final goal of this research is the layer-by-layer fabrication of functional gradient materials (3D parts) via the SLS method-6 using the feedback from the thermocouple measurements to control and guide the process. Comparative studies of the sintered microstructures and their element analysis shows not only the possibility of fabrication of intermetallic phases, but also to maintain, during laser controlled synthesis the degree of chemical transformation which under optimum conditions can reach up to 100%.

Acknowledgements

Authors thank the Russian Foundation of Fundamental Researches (grants Nos. 06-08-00102-a, 06-03-32119-a, 07-08-12048-ofi). IPP thanks the Royal Society Wolfson Trust for a merit award.

References

1 I. V. Shishkovskii, M. V. Kuznetsov, Yu. G. Morozov and I. P. Parkin, J. Mater. Chem., 14 (2004) 3444.
2 M. Yasuoka, Y. Nishimura, T. Nagaoka and K. Watari, J. Therm. Anal. Cal., 83 (2006) 407.
3 M. V. Kuznetsov, I. P. Parkin, A. Kvick, S. M. Busurin, I. V. Shishkovski and Yu.G. Morozov. Mater. Sci. Forum, 518 (2006) 181.
4 I. V. Shishkovsky, Rapid Prototyping J., 7 (2001) 207.

5 I. V. Shishkovsky, A. G. Makarenko and A. L. Petrov, Comb. Expl. Shock Waves, 35 (1999) 166.
6 D. M. Gureev, A. L. Petrov and I. V. Shishkovsky, The 6th International Conference on Industrial Lasers and Laser Applications '98, Vladislav Y. Panchenko; Vladimir S. Golubev; Eds, Proc. SPIE, 3688 (1999) 237.
7 A. V. Kamashev, A. C. Panin, A. L. Petrov and I. V. Shishkovsky, Lett. J. Techn. Phys. (JTP), 27 (2001) 28. (in Russian)
8 I. V. Shishkovsky, Yu. G. Morozov, A. C. Panin, S. E. Zakiev and M. V. Kuznetsov, Materiavolovedenie (Mater. Sci.), 3 (2003) 45. (in Russian)
9 E. Y. Tarasova, G. V. Kryukova, A. L. Petrov and I. V. Shishkovsky, Laser Applications in Microelectronic and Optoelectronic Manufacturing V, Henry Helvajian; Koji Sugioka; Malcolm C. Gower; Jan J. Dubowski; Eds., Proc. SPIE, 3933 (2000) 502.
10 I. V. Shishkovsky, A. L. Petrov and V. I. Scherbakov, Phys. Chem. Mater. Treatment, 3 (2001) 45. (in Russian)
11 I. V. Shishkovsky, M. V. Kuznetsov and Yu. G. Morozov, Glass Ceram., 60 (2003) 14. (in Russian)
12 I. V. Shishkovsky and Yu. G. Morozov, Proc. Samara Scientific Center of RAS, 6 (2004) 81. (in Russian)
13 V. V. Bagrov, N. A. Klimov, S. V. Nefedov, A. L. Petrov, V. I. Scherbakov and I. V. Shishkovsky, Proc. Samara Scientific Center of RAS, 5 (2003) 55. (in Russian)
14 S. E. Zakiev, L. P. Kholpanov, I. V. Shishkovsky, I. P. Parkin, M. V. Kuznetsov and Yu.G. Morozov, Appl. Phys. A, 84 (2006) 123.
15 P. Staszczuk, M. Błachnio, E. Kowalska and D. Sternik, J. Therm. Anal. Cal., 86 (2006) 51.
16 M. Barczak, J. Therm. Anal. Cal., 79 (2005) 499.

Received: January 24, 2007
Accepted: May 17, 2007
OnlineFirst: October 13, 2007

DOI: 10.1007/s10973-007-8353-8